Comparison of the Photocatalytic and Photoelectrocatalytic Decolorization of Methyl Orange on Sputtered TiO_2 Thin Films

Yuh-Fan Su and Tse-Chuan Chou

Department of Chemical Engineering, National Cheng Kung University, Tainan 701, Taiwan

Reprint requests to Prof. Dr. Tse-Chuan Chou. Fax: 886-6-2366836.
E-mail: tcchou@mail.ncku.edu.tw

Z. Naturforsch. **60b,** 1158 – 1167 (2005); received July 15, 2005

Correlations between the photocatalytic and photoelectrocatalytic decolorization of methyl orange, using TiO_2 thin films sputtered under various conditions, were made. Three types of systems, namely: two photocatalytic systems, one with and one without a Pt counter electrode, and a third with a Pt counter electrode having an applied potential, were used to evaluate photocatalytic activity.

The crystal structure, morphology, bandgap energy, flatband potential, and the resistances of the TiO_2 films were characterized by X-ray diffraction, scanning electron microscopy, UV/vis spectroscopy, a photocurrent method, and electrochemical impedance spectroscopy, respectively. The results showed that the decolorization of methyl orange only occurred on the anode of the TiO_2/Ti electrode and that the decolorization rate increased 67% when the photocatalyst was coupled to a Pt electrode (0 V applied potential), and 275% when connected with the Pt cathode and 1 V *vs.* Ag/AgCl applied potential. The benefits of high crystallinity, a high quantity of the anatase, and a more negative flatband potential were found in the photocatalytic reaction, whereas the resistance of the film was the main factor affecting the photoelectrocatalytic activity.

Key words: Titanium Dioxide, Methyl Orange, Sputtering, Photoelectrocatalytic Activity, Photocatalytic Decolorization

Introduction

Metal oxide semiconductor photocatalysts have recently attracted attention because of their potential application to the purification and treatment of air and water as well as solar energy conversion and storage [1 – 7]. Among the photocatalysts, TiO_2 is the most promising material due to its non-toxicity, good long-term stability, and low price [8 – 12].

Photoelectrochemical cells are constructed as semiconductor photocatalysts are immobilized on a conductive substrate and connected with a counter electrode. When an appropriate potential is applied, a depletion layer is formed on the surface of the semiconductor at the interface with the solution. This depletion layer decreases the recombination of photo-excited electron-hole pairs resulting in a significantly increased photo-efficiency. When holes in TiO_2 are conducted to the surface of the semiconductor and electrons are transferred from the conductive substrate through an external circuit to the counter electrode, a measurable current will arise from photo-irradiation. As the reactions of electrons and holes are at different electrodes, the problem of product separation is avoided. Due to the advantages mentioned above, the application of the photoelectrocatalytic system has been studied extensively [13 – 18].

Several researches have explored the relationship between material behavior and the photocatalytic activity of photocatalysts in order to obtain the best light energy conversion efficiency [19 – 23]. However, most of the studies have focused on the photocatalytic activity of TiO_2 powders or thin films in the absence of an applied potential. For the photocatalytic reaction in the presence of an applied potential, only a few researchers have investigated the correlation between material behavior and photoelectrocatalytic activity. M. Takahashi reported that the photocurrent density was influenced by the thickness of TiO_2 thin films prepared by the sol-gel method [24]. T. V. Nguyen has worked out the effect of flatband potential of the TiO_2 film prepared by the sol-gel method on the photocurrent density [25]. F. Gracia discussed the relationship between the microstructure and the photocurrent density of TiO_2 films prepared by the CVD method [26]. In our previous work, the effect of the microstructure

Table 1. Reactive sputtering conditions for preparing TiO_2 films and summary of their resulting properties.

	— Sputtering condition —						
Sample	Oxygen mole [%]	Total pressure [10^{-2} mbar]	Sputtering power [W]	Grain size (D_g) [nm]	Bandgap energy (E_{bg}) [eV]	Flatband potential (V_{fb}) [V]	Resistance (R_f) [Ω cm^2]
1	20	1.6	100	29	3.27	**−0.29**	**789**
2	100	1.6	100	36	3.21	−0.15	380
3	20	6.4	100	31	3.25	−0.21	454
4	100	6.4	100	25	3.29	−0.14	315
5	20	1.6	210	42	3.19	−0.01	*27*
6	100	1.6	210	33	3.23	*−0.01*	92
7	20	6.4	210	**49**	*3.10*	-0.24	583
8	100	6.4	210	*22*	**3.30**	-0.18	227

of the sputtered TiO_2 film on the photocurrent density was investigated [27].

The effect of the applied potential on the photocatalytic activity was found to be quite significant. The photocatalytic activity was increased by applying a potential [16 – 18]; semiconductors that do not have any photocatalytic activity, however, can have photoelectrocatalytic activity [13 – 15]. This implies that the photoactivity strongly depends on material properties as well as on the presence and absence of an applied potential. However, our knowledge of the influence of a material's electric properties on the photoelectrocatalytic reaction system is still very limited. A detailed investigation of material properties in the presence and absence of an applied potential is also necessary to evaluate appropriate photocatalysts for further application.

Photocurrent cannot be directly measured from photocatalytic reactions. In order to compare the activities of photocatalysts under the conditions of photocatalytic and photoelectrocatalytic reactions, the rate of reactant disappearance was measured. Methyl orange (MO), a typical azo dye, was chosen as our model compound since MO is a serious pollutant in textile wastewater [28]. The rate of decolorization of MO was monitored and used to evaluate the activity of photocatalytic and photoelectrocatalytic reactions in this work. TiO_2 thin films with various characteristics were deposited onto a Ti plate using reactive sputtering. The sputtering technique allows the fabrication of large-scale uniform coatings which have good adhesion to substrates at relatively low substrate temperatures [29].

Material properties including: crystal structure, morphology, bandgap energy, flatband potential, and the resistance of the TiO_2 films were characterized. The relationships of various material properties to photocatalytic and photoelectrocatalytic activities are discussed. In addition, the photocurrent was measured to compare the different methods used to evaluate the photoelectrocatalytic activity including the rate of decolorization and photocurrent density. The photocurrent efficiency of photoelectrocatalytic decolorization of MO was also evaluated.

Experimental Section

Sample preparation

TiO_2 film was deposited on a titanium metal target (5.08 cm diameter, 99.7% purity, Target Materials, Inc.) in an argon-oxygen atmosphere by controlling preparation factors including oxygen mole percentage, total pressure, and sputtering power. The setting of sputtering conditions is shown in Table 1. The deposition time was controlled for different sputtering conditions to obtain the same thickness of 500 nm. The details of the sputtering procedure were described in a previous study [27]. All TiO_2 thin films were used directly after sputtering without further calcination. The prepared electrode was partially sealed with Teflon tape to define the working electrode area of 12.25 cm^2. In addition, TiO_2 was deposited on Si wafers in order to accurately measure the thickness of the film because the thickness measurement at a Ti substrate was limited by a hackly surface.

Film characterization

A surface profilometer (Alpha-Step 200, Tencor) was used to measure the thickness of the TiO_2 films. The crystal structure of the TiO_2 films was analyzed using XRD with a Cu-K_α radiation source. The applied current and voltage of the X-ray diffractometer (D/max3.V, Rigaku) were 30 mA and 40 kV, respectively. The patterns obtained were identified according to the PCPDFWIN Powder Diffraction File (International Center for Diffraction Data). The morphology of the film was investigated using high-resolution analysis electron microscopy (SEM, S4100, Hitachi). Before SEM was carried out, a Pt thin film was sputtered onto the sample to prevent charge build up. The mean particle size was obtained by measuring 100 particles in a specified area. The UV/vis absorption spectrum of the TiO_2 film was measured by the diffuse

reflection method using a spectrophotometer (Jasco 7850, Japan Spectroscopic Co., Ltd.) equipped with an integrating sphere (TIS-417). The resistance of TiO_2 films was measured using electrochemical impedance spectroscopy (614A, CH Instruments) at 1 kHz. The TiO_2/Ti electrode, a Pt counter electrode, and a $Ag/AgCl_{KCl(sat'd)}$ reference electrode were immersed in a 0.1 M aqueous $NaClO_4$ electrolyte solution. The cell electrolyte was open to air and stayed quiescent during experimental procedures.

Photocatalytic and photoelectrocatalytic activities measurement

The photocurrent was measured in a classical three-electrode electrochemically divided cell irradiated by a 800 W super-high-pressure Hg(Xe) Lamp (68820 universal power supply and 66020 lamp housing, Oriel) combined with a potentiostat/galvanostat (273A, EG&G) as shown in Fig. 1a. The cell was kept at 30 °C by using a cooling jacket and set at a distance of 6 cm from the irradiation lamp. The TiO_2/Ti electrode was used as the working electrode, the counter electrode was a Pt plate (1×1 cm^2), and the reference electrode was a $Ag/AgCl_{KCl(sat'd)}$ electrode. The supporting electrolyte was aerated 0.1 M aqueous $NaClO_4$. The incident light intensity was measured using a radiometer (SEL005, IL1400A, International light). The photocurrent-voltage characteristic of the electrode was determined by linear sweep voltammetry from -0.75 to 3.25 V *vs.* Ag/AgCl with a scan rate of 50 mV s^{-1}.

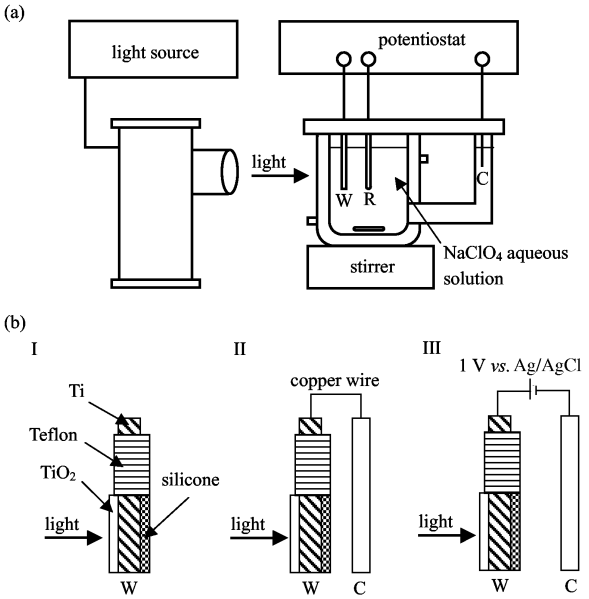

Fig. 1. (a) Photoelectrocatalytic reactor design. (b) Three types of measurement conditions for decolorization reaction. W: TiO_2/Ti electrode; C: Pt plate; R: Ag/AgCl electrode.

The apparatus for photocurrent measurement was also used for the photocatalytic MO decolorization reaction. MO was added to the $NaClO_4$ electrolyte until the total concentration of MO was 7×10^{-5} M. The TiO_2/Ti electrode was then immersed into the solution. After saturated adsorption of MO on the surface of the TiO_2 film, a photocatalytic reaction was carried out by light irradiation. The reduction in the MO concentration was determined as a function of reaction time by an UV/vis spectrophotometer (Jasco) at 465 nm wavelength. Samples were periodically taken from the reactor with a pipette that did not permit feed-back into the solution. The pH of sampled MO was adjusted to be > 5.0 by the addition of a NaOH solution.

The photocatalytic activity of the TiO_2 thin films was evaluated by the decolorization rate measured by MO concentration change during the initial reaction period. Three types of conditions for the photocatalytic reactions are depicted in Fig. 1b. In the first type (1b, I), the TiO_2/Ti electrode was only exposed to light and the photocatalytic reaction rate measured in this way was defined as Ri_{TiO_2}. In the second type (1b, II), the TiO_2/Ti electrode connected with a Pt plate was exposed to light and Ri_{TiO_2-Pt} was used to determine the photocatalytic reaction rate. In the third type (1b, III), a 1 V *vs.* Ag/AgCl potential was applied to the TiO_2/Ti electrode connected with a Pt plate and the photocatalytic reaction rate measured, this system was defined as Ri_{TiO_2-Pt+E}. The third system was also a photoelectrochemical cell. In this system, photocurrent efficiency was defined as the ratio of photo-generated current related to the decolorization of MO [14],

$$\varepsilon_R = nFR_i/I_R \times 100\%, \quad (1)$$

where n is the number of electrons per molecule oxidized or reduced (which is 2 for the decolorization of MO [30]), F the Faraday constant (96500 C), R_i (in mol m^{-2}s^{-1}) the initial decolorization reaction rate and I_R (in A m^{-2}) the photocurrent density.

Results and Discussion

Film characterization

Crystal structure

XRD patterns of TiO_2 thin films prepared by different reactive sputtering conditions are shown in Fig. 2. The diffraction peak positions (2θ) at 25.4, 48.1, and 53.90 refer to the (101), (200), and (105) planes of anatase respectively, while the diffraction peaks at 27.5, 36.1, and 54.30 correspond to the (110), (101), and (211) planes of rutile. The peaks of the Ti support substrate also appear due to the thinness of the TiO_2 films.

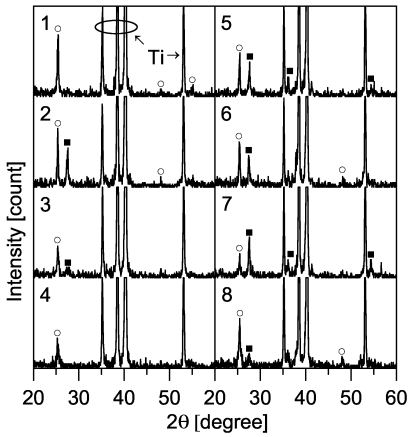

Fig. 2. The XRD patterns of TiO_2 films. ○: anatase; ■: rutile.

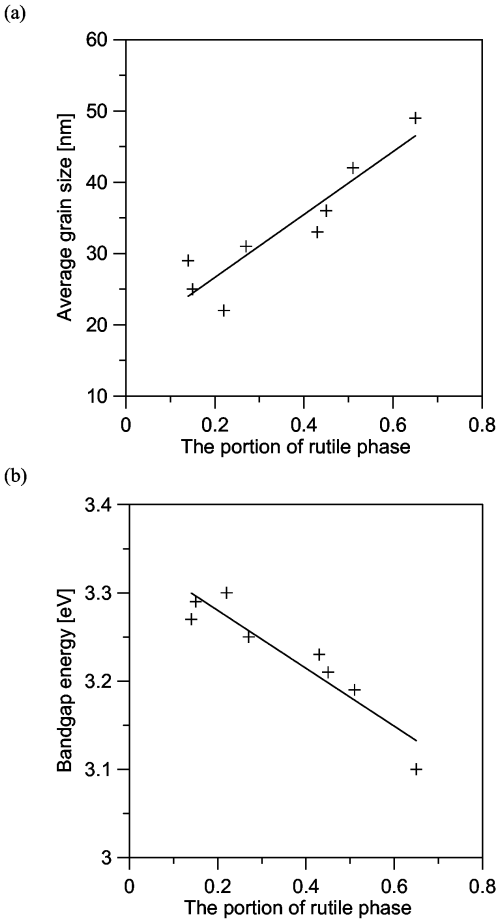

Fig. 3. The relationship between (a) the average grain size, (b) the bandgap energy, and the portion of rutile phase. A and R are the diffraction peak areas of anatase and rutile, respectively, quantified from XRD patterns as shown in Fig. 2.

The results indicated that sputtered TiO_2 films had good crystallinity even without calcination. All of the prepared TiO_2 thin films contained both anatase and rutile phases, with anatase being dominant in most samples. In our previous study, TiO_2 was sputtered on ITO substrates and we derived the anatase-rutile phase transformation diagram at different sputtering powers and total pressures [27]. When compared with the sputtered TiO_2 on Ti substrate in this study, the portion of rutile phase formed was more than that of the sputtered TiO_2 on ITO using the same sputtering conditions.

Samples 3 and 4 had relatively poor crystallinity, due to the application of low sputtering power providing low kinetic energy to the particles, while high pressure further increased the energy lost from the interactions of particles during collisions. Therefore, when the sputtered particles arrived at the surface of the substrate, they lacked the mobility needed for efficient crystallization.

The average grain size was obtained from Scherrer's equation [31] as shown in Table 1. Fig. 3a shows the relationship between average grain size and the portion of rutile phase. The average grain size increased from 22 to 49 nm while the portion of rutile phase increased from 22 to 65%. Because rutile is the thermally stable polymorph compared with anatase it was formed when sufficient energy was present to enable the particles to grow.

Surface morphology

The SEM images of the TiO_2 thin films sputtered on Ti substrates are shown in Fig. 4. From surface observations, the film was constructed from many tiny particles with loose structures and intervening spaces. This morphology was very similar to the sputtered TiO_2 film on the ITO substrate [27]. Two structures can form on the film. One type is constituted from the tiny particles closely piled up; the other is the column-shape structure which grows perpendicular to the surface of the substrate [32 – 34]. These two structural formations are compact in the interior of the thin layer (from the side view) and are not like the loose forms observed in the top view. The particle sizes varied in the range from 30 to 100 nm with different sputtering conditions. Compared with the average grain sizes calculated from XRD, most of the particles observed in SEM were primary grains.

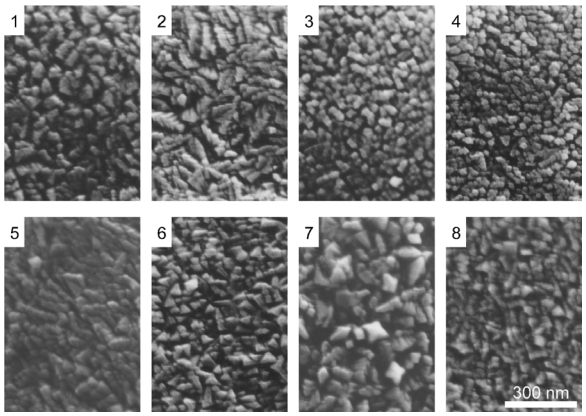

Fig. 4. The SEM images of TiO_2 films.

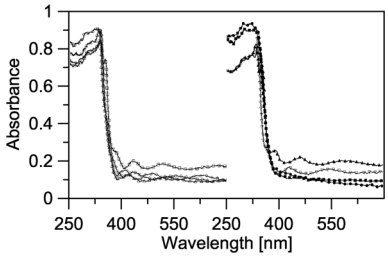

Fig. 5. The UV/vis absorption spectra of TiO_2 films. ◊: sample 1; □: sample 2; ○: sample 3; △: sample 4; ▽: sample 5; ▲: sample 6; ●: sample 7; ■: sample 8.

Bandgap energy

Fig. 5 shows the UV/vis absorption spectra of TiO_2 films. Different sputtering conditions did not obviously influence the UV/vis absorption spectra of the TiO_2 films, with the main absorption band remaining in the ultraviolet range. The bandgap energy, as listed in Table 1, was estimated by plotting $(\alpha h\nu)^{1/2}$ *versus* $h\nu$ for TiO_2 which corresponds to the indirect transition, where α is the absorption coefficient and $h\nu$ is the photon energy [35]. The bandgap energy depended on the crystal phase transformation of the film. The relationship between the bandgap energy and the portion of the rutile phase is depicted in Fig. 3b. The bandgap energy was decreased from 3.3 to 3.1 eV when the portion of rutile phase increased from 22 to 65%. The value of the bandgap energy obtained in this study was a little higher than that reported in the literature [36]. A semiconductor with lower bandgap energy absorbs more photo-energy.

Flatband potential

Fig. 6 shows the photocurrent-voltage (I_{pc}-E) curves of TiO_2/Ti electrodes in the presence and absence of ir-

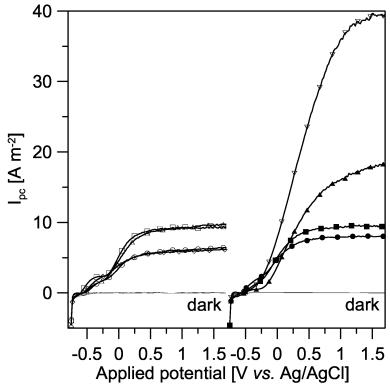

Fig. 6. I_{pc}-E curves of TiO_2/Ti electrodes in the presence and absence of the irradiation. ◊: sample 1; □: sample 2; ○: sample 3; △: sample 4; ▽: sample 5; ▲: sample 6; ●: sample 7; ■: sample 8.

radiation. There was no photocurrent while the light was turned off. The measured photocurrent was induced from the photo-excitation of electrons and holes. The sputtered TiO_2 film had photocatalytic activity even without additional calcination. The photocurrent was increased in the presence of an applied anodic potential and approached a steady value above 1 V *vs.* Ag/AgCl.

The flatband potential, as listed in Table 1, was determined from the I_{pc}^2 *versus* E plot [37]. The flatband potential of the sputtered TiO_2 film was in the range from -0.14 to -0.29 V *vs.* Ag/AgCl for most samples. The value of the flatband potential for samples 5 and 6 was -0.01 V *vs.* Ag/AgCl, smaller than for other samples. This was attributed to the influence of crystal morphology and the bulk or surface composition [38]. Literature values for the flatband potential of TiO_2 are in the range from -0.1 to -0.8 V *vs.* SCE at pH 5.5 [39]. Different values of the flatband potential are due to different methods of preparation and measurement as well as to the electrolyte composition.

Film resistance

In order to compare the transfer resistance of electrons from the surface to the conductive substrate in different films, the resistance of the thin films was measured as shown in Table 1. The electron transfer resistance of sample 5 was the smallest and that of sample 1 was the largest. The different resistance obtained here was mainly attributed to different grain boundary barriers arising from microstructure change [40, 41].

Table 2. Photocatalytic and photoelectrocatalytic activities of TiO_2 films evaluated by photocurrent measurement and decolorization rate of MO.

Sample	I_{pc} [Am^{-2}]	R_i [$\mu mol\,m^{-2}s^{-1}$]			I_R [$A\,m^{-2}$]	ε_R [%]
		TiO_2	TiO_2-Pt	TiO_2-Pt+E		
1	*5.87*	0.11	0.17	0.19	*0.93*	3.91
2	9.27	0.09	0.16	0.31	1.67	3.53
3	6.02	0.05	*0.09*	*0.15*	1.06	2.78
4	9.35	0.08	0.11	0.28	1.61	3.41
5	**36.00**	0.03	0.18	**0.68**	**9.31**	*1.42*
6	16.08	*0.02*	**0.22**	0.64	5.70	2.17
7	7.93	**0.12**	0.21	0.35	1.53	**4.46**
8	9.35	0.09	0.14	0.36	1.68	4.14

I_{pc}: the photocurrent density measured in the absence of MO; Ri: the initial reaction rate of decolorization of MO; Ri_{TiO_2}, Ri_{TiO_2-Pt}, and Ri_{TiO_2-Pt+E} were obtained by three types of measurement conditions for decolorization of MO as shown in Fig. 1b; I_R: the photocurrent density measured in the presence of MO; ε_R: the photocurrent efficiency.

Photocatalytic and photoelectrocatalytic decolorization of MO

Two blank experiments were carried out: (a) MO was illuminated by ultraviolet only, and (b) the TiO_2/Ti electrode was used to electrolyze MO in the presence of an applied potential of 1 V *vs.* Ag/AgCl. The results showed that MO was not decolorized, neither by irradiation from a UV light source nor by applying a potential on the TiO_2/Ti electrode. The decolorization of MO was only observed by using the TiO_2/Ti electrode in the presence of the UV irradiation needed to carry out a photocatalytic reaction. Additionally, this reaction only occurred on the anode of the TiO_2/Ti electrode, as there was not any color change on the Pt cathode. This indicated that the decolorization of MO resulted from a series of reactions caused by the photoexcited holes. During the photocatalysis, OH radicals are generated and contribute to the decomposition of organic species [42].

The photocatalytic activities Ri_{TiO_2}, Ri_{TiO_2-Pt}, and Ri_{TiO_2-Pt+E} measured for three types of systems are listed in Table 2. The photocurrent density I_{pc} obtained from Fig. 6 at an applied potential of 1 V, I_R obtained in the type III, and the photocurrent efficiency (ε_R) calculated through Ri_{TiO_2-Pt+E} and I_R from eq. (1) are also listed in Table 2.

The average Ri_{TiO_2} was found to be 0.07 $\mu mol\,m^{-2}s^{-1}$ for variously sputtered TiO_2 thin films. With the film connected with the Pt plate, the average Ri_{TiO_2-Pt} increased by 67% to 0.16 $\mu mol\,m^{-2}s^{-1}$. It has been reported that the improvement of the photocatalytic efficiency by Pt deposited on a TiO_2 photocatalyst is mainly due to (i) the high electron affinity and hence increased lifetime of the excitons, thus slowing the recombination of the electron-hole pairs and (ii) the promotion of the dissociative adsorption of hydrogen as H_{ads} for metals with low H^+/H_2 potential [43]. An applied potential of 1 V *vs.* Ag/AgCl further increased Ri_{TiO_2-Pt+E} to 0.37 $\mu mol\,m^{-2}s^{-1}$, and the average increased by 127%. Totally, connecting with Pt at 1 V *vs.* Ag/AgCl applied potential increased the decolorization rate by 275% in average compared with the original system.

The highest values of Ri_{TiO_2} and ε_R were obtained with the sample 7. The sample 6 had the lowest Ri_{TiO_2} but the highest Ri_{TiO_2-Pt}. The sample 5 had the highest I_{pc}, Ri_{TiO_2-Pt+E}, and I_R, but its ε_R was the lowest. Different photocatalytic activities of a TiO_2 film were obtained when different experimental methods were used. This discrepancy in the photocatalytic activities of TiO_2 films was caused by various properties of the materials prepared by different sputtering conditions. The detailed correlation between the photocatalytic activity and the material properties will be discussed below.

The values of I_{pc} were proportional to the values of I_R, as shown in Fig. 7; notably, all I_{pc} values were larger than I_R values. In the decolorization reaction of MO, a portion of incident light was shadowed by MO and the actual light intensity reaching the surface of the TiO_2 thin-film was decreased.

Fig. 7 also shows the relationship between the Ri_{TiO_2-Pt+E} and I_{pc} to allow a comparison of the methods for measuring photoelectrocatalytic activities with various samples. I_{pc} was contributed from the effective

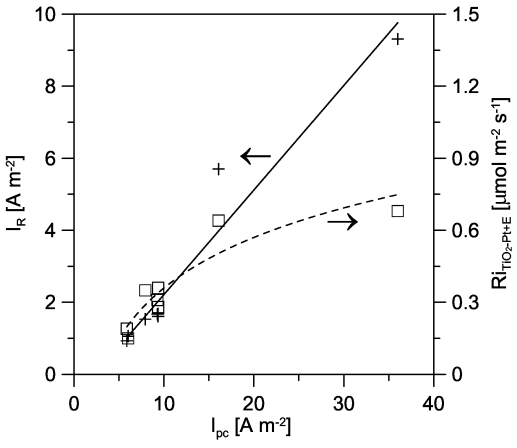

Fig. 7. The relationship between the I_R, Ri_{TiO_2-Pt+E}, and I_{pc}.

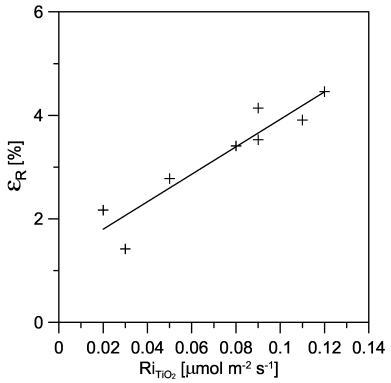

Fig. 8. The relationship between ε_R and Ri_{TiO_2}.

separation of photo-excited electron-hole pairs. Only a part of the photocurrent was involved in the decolorization of MO. The portion of photocurrent acting on the decolorization of MO (ε_R) depended on the surface properties of the TiO_2 films. The values of ε_R were not constant but fell in the range from 1.42 to 4.46%. Therefore, the photoelectrocatalytic activities obtained in these two ways were not the same.

Fig. 8 shows the values of Ri_{TiO_2} *versus* ε_R obtained from various samples. As Ri_{TiO_2} increased from 0.03 to 0.12 μmol m^{-2}s^{-1}, ε_R increased from 1.42 to 4.46%, indicating that TiO_2 films had higher activity in the photocatalytic reaction in the absence of the applied potential; while, in the photoelectrocatalytic reaction in the presence of an applied potential they have a higher selectivity for the decolorization of MO.

Photocatalytic and photoelectrocatalytic activities correlated to characteristics of the TiO$_2$ thin films

Crystal structure

In photocatalytic reactions, it is generally acknowledged that crystalline TiO_2 has a higher photocatalytic activity than the amorphous form. The photocatalytic activity of the anatase phase is better than that of rutile [19]. Samples 5 and 6 which had the best photoelectrocatalytic activity were significantly crystalline in nature; nevertheless, their crystalline composition contained a significant quantity of rutile. This suggests that the good crystallinity of TiO_2 was beneficial for the photoelectrocatalytic reaction. However, both the anatase and rutile crystal phases show similar photoelectrocatalytic activities in the presence of the applied potential. This was attributed to the low photocatalytic activity of rutile caused by the high recombination ratio of electron-hole pairs which could be restrained by applying a potential [13, 14]. Therefore, the rutile phase TiO_2 exhibited good photoelectrocatalytic activity in the presence of the applied potential.

Surface morphology

In general, films with smaller particle sizes have a larger surface area available for reaction; therefore, for most catalytic reactions, the catalyst that has the highest surface gives the fastest reaction rate. But in this study, the reaction rate was not apparently directly related to the particle sizes of the films for either the photocatalytic or the photoelectrocatalytic reactions, because these reactions were initiated by light. For the film type photocatalysts, the particle size in the film did not affect significantly the real illuminated area which leads to a similar photoactivity.

Flatband potential

The Fermi level of the photocatalyst, which represents the reduction ability of the photo-excited electron can be evaluated from the flatband potential [44]. The samples which possessed a more negative flatband potential and with photo-excited electrons had a higher reduction ability than the samples possessing a more positive flatband potential. When the flatband potential was increased from -0.24 to -0.01 V, Ri_{TiO_2} decreased from 0.12 to 0.02 μmol m^{-2}s^{-1} as shown in Fig. 9. When TiO_2 was connected with Pt, the flatband potential effect became insignificant with respect to both the photocatalytic activity of Ri_{TiO_2-Pt} and the photoelectrocatalytic activity of Ri_{TiO_2-Pt+E} (see the seventh column in Table 1, and the fourth and fifth

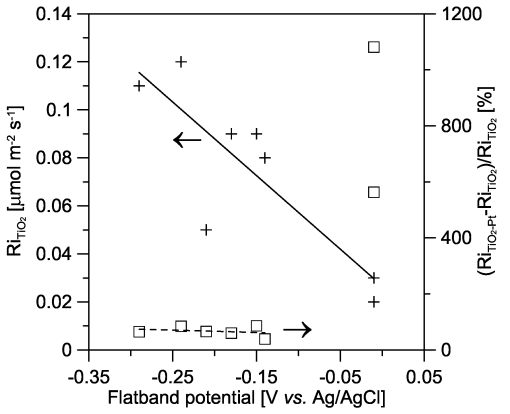

Fig. 9. The relationship between Ri_{TiO_2}, $(Ri_{TiO_2-Pt}–Ri_{TiO_2})/Ri_{TiO_2}$, and flatband potential.

columns in Table 2). This was because Pt can reduce the H^+/H_2 potential and electrons are able to produce hydrogen.

The relationship between the increase of the decolorization rate after the TiO_2/Ti electrode was connected with a Pt plate and the flatband potential is also shown in Fig. 9. The photocatalytic activity of samples 5 and 6 was raised 5.6 and 10.8-fold, respectively, after connecting to Pt. However, the photocatalytic activity of other samples only increased in the range from 39 to 86% when connecting to Pt. This suggests that the flatband potential of samples 5 and 6 were too positive to cause hydrogen evolution without Pt. But the reaction still took place on other samples even though the rate was not high. Therefore, samples 5 and 6 connected with Pt resulted in relatively large increases in photocatalytic activity.

Film resistance

As shown in Fig. 10, while the film resistance increased from 27 to 789 Ω cm^2, the photocatalytic decolorization rate by a fixed applied potential of 1 V *vs.* Ag/AgCl decreased from 272 to 8%. As the film resistance increases, the applied potential should increase due to the increasing potential loss caused by the resistance of the film. On the other hand, the increase of the resistance of electrons transferring from the TiO_2 surface to the Ti substrate also increased the recombination of electron-hole pairs. The decrease of the film resistance had an obvious influence on the improvement of photocatalytic activity when a potential was applied.

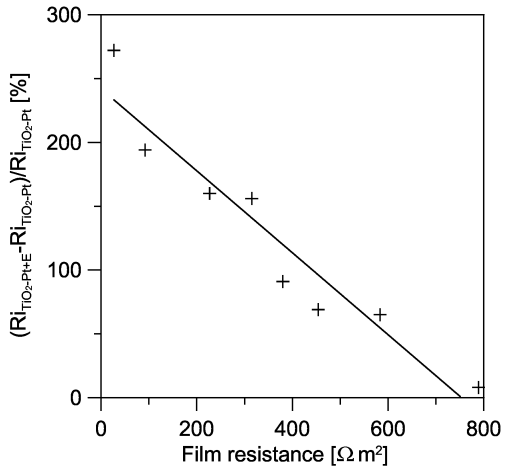

Fig. 10. The relationship between $(Ri_{TiO_2-Pt+E}-Ri_{TiO_2-Pt})/Ri_{TiO_2-Pt}$ and the film resistance.

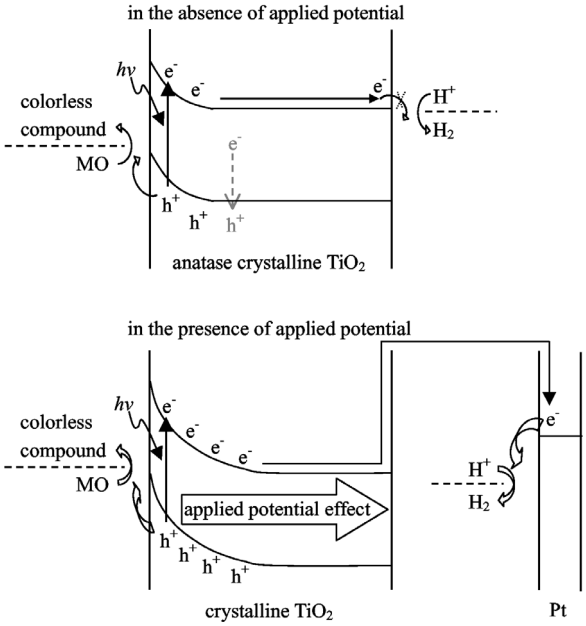

Fig. 11. Schematic diagrams representing the material effect on both photocatalytic and photoelectrocatalytic decolorization of MO.

The sample 1 had higher resistance (789 Ω cm^2) than the sample 8 (227 Ω cm^2). Sample 1 also had a larger photocatalytic activity than sample 8 but this order was reversed for photoelectrocatalytic activity.

To summarize the above: Fig. 11 illustrates the material effect on both the photocatalytic and photoelectrocatalytic decolorization of MO. When photo-excited holes oxidize H_2O or OH^- ions, strong oxidants *e.g.* OH· free radicals are produced, which are able to react with MO that is adsorbed on the surface of the TiO_2 film. The number of effective holes produced affects the decolorization rate of MO. In the photocatalytic reaction, high crystallinity, high quantity of anatase, and more negative flatband potential reduce the recombination of electron-hole pairs to obtain more holes and higher decolorization rates. However, in the photoelectrocatalytic reaction, the applied potential becomes the main force preventing the recombination of electrons and holes, rutile also has high photoelectrocatalytic activity and the quantity of anatase is not important. Decreasing the resistance of the film maximizes the effect of the applied potential and decreases the resistance of electron transfer. Therefore, the resistance of the film is the main factor affecting the photoelectrocatalytic activity. In addition, using Pt as the counter electrode reduces the H^+/H_2 potential and flatband po-

tential effects become insignificant for the photoelectrocatalytic reaction under these conditions. The photocatalytic and photoelectrocatalytic activities are affected by different material properties. Consequently, samples with good photocatalytic activity do not of necessity have good photoelectrocatalytic activity.

Conclusions

An analysis of the above work allows us to draw the following conclusions. The sputtered TiO_2 thin films had good crystallinity even without calcination and their average grain sizes were in the range from 22 to 49 nm. Both anatase and rutile phases were found in the prepared films. The values of the bandgap energy were in the range from 3.1 to 3.3 eV. The flatband potential of the sputtered TiO_2 film was in the range from -0.14 to -0.29 V *vs.* Ag/AgCl.

It was found that the decolorization of MO only occurred on the anode of the TiO_2/Ti electrode. The photocurrent efficiency was between 1.42 and 4.46%. TiO_2 films had higher activities in photocatalytic reactions in the absence of an applied potential, and also had a higher selectivity for the decolorization of MO in the presence of an applied potential. With the photocatalyst connected to a Pt plate, the average photocatalytic decolorization rate of MO increased by 67%. The decolorization rate further increased by 127% in the presence of an applied potential of 1 V *vs.* Ag/AgCl.

For the photocatalytic reaction, the material properties with high crystallinity, high quantity the anatase, and more negative flatband potential give a higher decolorization rate. For the photoelectrocatalytic reaction, the crystal phase was not important and the flatband potential effect was not affected when connected to Pt. However, the resistance of the film was the most important factor for determining the photoelectrocatalytic activity.

Acknowledgements

The support of the Ministry of Education of the Republic of China (EX-91-E-FA09-5-4), the National Science Council (NSC 93-2214-E-006-009), and National Cheng Kung University are gratefully acknowledged.

[1] A. Fujishima, K. Honda, Nature **238**, 37 (1972).
[2] L. C. Chen, T. C. Chou, J. Mol. Catal. A-Chem. **85**, 201 (1993).
[3] D. A. Tryk, A. Fujishima, K. Honda, Electrochim. Acta **45**, 2363 (2000).
[4] O. M. Alfano, D. Bahnemann, A. E. Cassano, R. Dillert, R. Goslich, Catal. Today **58**, 199 (2000).
[5] K. Rajeshwar, N. R. de Tacconi, C. R. Chenthamarakshan, Chem. Mater. **13**, 2765 (2001).
[6] K. Pirkanniemi, M. Sillanpaa, Chemosphere **48**, 1047 (2002).
[7] I. Salem, Catal. Rev.-Sci. Eng. **45**, 205 (2003).
[8] L. C. Chen, T. C. Chou, Ind. Eng. Chem. Res. **33**, 1436 (1994).
[9] M. I. Litter, J. A. Navio, J. Photochem. Photobiol. A-Chem. **98**, 171 (1996).
[10] M. Anpo, M. Takeuchi, J. Catal. **216**, 505 (2003).
[11] I. K. Konstantinou, T. A. Albanis, Appl. Catal. B-Environ. **49**, 1 (2004).
[12] O. Carp, C. L. Huisman, A. Reller, Prog. Solid State Chem. **32**, 33 (2004).
[13] C. C. Sun, T. C. Chou, Ind. Eng. Chem. Res. **37**, 4207 (1998).
[14] C. C. Sun, T. C. Chou, J. Mol. Catal. A-Chem. **151**, 133 (2000).
[15] J. Luo, M. Hepel, Electrochim. Acta **46**, 2913 (2001).
[16] H. Liu, S. A. Cheng, M. Wu, H. J. Wu, J. Q. Zhang, W. H. Li, C. N. Cao, J. Phys. Chem. A **104**, 7016 (2000).
[17] S. U. M. Khan, M. Al-Shahry, W. B. Ingler, Science **297**, 2243 (2002).
[18] P. A. Christensen, T. P. Curtis, T. A. Egerton, S. A. M. Kosa, J. R. Tinlin, Appl. Catal. B-Environ. **41**, 371 (2003).
[19] S. Ichikawa, R. Doi, Thin Solid Films **292**, 130 (1997).
[20] H. Fujii, M. Ohtaki, K. Eguchi, J. Am. Chem. Soc. **120**, 6832 (1998).
[21] R. Asahi, T. Morikawa, T. Ohwaki, K. Aoki, Y. Taga, Science **293**, 269 (2001).
[22] T. Kawahara, Y. Konishi, H. Tada, N. Tohge, J. Nishii, S. Ito, Angew. Chem. Int. Ed. **41**, 2811 (2002).
[23] S. I. Shah, W. Li, C. P. Huang, O. Jung, C. Ni, Proc. Natl. Acad. Sci. U. S. A. **99**, 6482 (2002).
[24] M. Takahashi, K. Tsukigi, T. Uchino, T. Yoko, Thin Solid Films **388**, 231 (2001).
[25] T. V. Nguyen, O. B. Yang, Catal. Today **87**, 69 (2003).
[26] F. Gracia, J. P. Holgado, A. R. Gonzalez-Elipe, Langmuir **20**, 1688 (2004).
[27] Y. F. Su, T. C. Chou, T. R. Ling, C. C. Sun, J. Electrochem. Soc. **151**, A1375 (2004).
[28] H. Destaillats, A. J. Colussi, J. M. Joseph, M. R. Hoffmann, J. Phys. Chem. A **104**, 8930 (2000).

[29] S. J. Nadel, P. Greene, J. Rietzel, J. Strumpfel, Thin Solid Films **442**, 11 (2003).
[30] L. C. Chen, T. C. Chou, Ind. Eng. Chem. Res. **32**, 1520 (1994).
[31] B. D. Cullity, S. R. Stock, Elements of x-ray diffraction, third ed., Prentice Hall, Upper Saddle River, NJ (2001).
[32] J. Szczyrbowski, G. Brauer, M. Ruske, G. Teschner, A. Zmelty, J. Non-Cryst. Solids **218**, 262 (1997).
[33] A. Yasumori, H. Shinoda, Y. Kameshima, S. Hayashi, K. Okada, J. Mater. Chem. **11**, 1253 (2001).
[34] M. J. Jung, Y. M. Kim, Y. M. Chung, J. G. Han, K. Y. Bang, Thin Solid Films **447**, 430 (2004).
[35] J. I. Pankove, Optical processes in semiconductors, chapter 3, Dover Pub., New York (1971).
[36] N. Serpone, in E. Pelizzetti (ed.): Photocatalysis: fundamentals and applications, Wiley, New York (1989).
[37] J. Akikusa, S. U. M. Khan, Int. J. Hydrog. Energy **22**, 875 (1997).
[38] H. O. Finklea, in H. O. Finklea (ed.): Semiconductor electrodes, p. 1 – 42, Elsevier, New York (1988).
[39] H. O. Finklea, in H. O. Finklea (ed.): Semiconductor electrodes, p. 43 – 145, Elsevier, New York (1988).
[40] C. W. Nan, A. Tschope, S. Holten, H. Kliem, R. Birringer, J. Appl. Phys. **85**, 7735 (1999).
[41] A. Rothschild, Y. Komem, A. Levakov, N. Ashkenasy, Y. Shapira, Appl. Phys. Lett. **82**, 574 (2003).
[42] O. M. Alfano, M. I. Cabrera, A. E. Cassano, J. Catal. **172**, 370 (1997).
[43] A. V. Vorontsov, I. V. Stoyanova, D. V. Kozlov, V. I. Simagina, E. N. Savinov, J. Catal. **189**, 360 (2000).
[44] A. J. Zozik, in F. Cardon, W. P. Gomes, W. Dekeyser (ed.): Photovoltaic and photoelectrochemical solar energy conversion, p. 263 – 310, Plenum Press, New York (1981).